25th ABCM International Congress of Mechanical Engineering
October 20-25, 2019, Uberlândia, MG, Brazil

# COB-2019-0012
# INFLUENCE OF REYNOLDS NUMBER IN THE REGION OF FLOW DEVELOPMENT IN BIFURCATIONS

**Flavio Peres Amado**
Universidade Estacio de Sá, Rua Eduardo Luiz Gomes, 134 - Morro do Estado, Niterói - RJ, 24020-340
e-mails: flavioam@petrobras.com.br; fpamado@live.estacio.com.br
**Victor Hugo Mondaini Corradi**
**Pablo Ferdandes Henriquez Vergara**
**Narcisio Gregory dos Santos Mazzarela**
**Wesley de Abreu da Silva**
Universidade Estacio de Sá, Rua Eduardo Luiz Gomes, 134 - Morro do Estado, Niterói - RJ, 24020-340
e-mails: vic.hugmondaini@yahoo.com.br; pablofhvergara@gmail.com; narcisio.gregory@gmail.com; wees.abreu@gmail.com

***Abstract.*** *The region of flow development in bifurcation was studied in previous works presented by the author in the events CONEM 2018 and ENCIT 2018. The objective was to find an expression that could predict the length, as a function of flow parameters, channel dimensions and fork angles. At this point, the aim is to advance in the state of the art by checking the influence of the Reynolds number on the extension of that region, varying the viscosity and the density of the fluid, keeping the flow rate constant. The equations proposed in the aforementioned manuscripts were tested by comparing the calculated values with those raised employing a CFD technique, which used the finite difference method as well as a commercial package. The results obtained allow to conclude that the proposed equation for prediction of lengths as a function of the flow rate was better suited to the majority of the simulation results than the wide aspect equation, except for low-viscosity hydraulic oils where the broad-spectrum equation behaved a little better. The present work concludes a study cycle of the developing flow region in bifurcations and the results achieved shall be used in future models for predicting the extension of the thermal developing region.*

***Keywords:*** *Reynolds Number, Flow Development, Bifurcations*

## 1. INTRODUCTION

Classically, it is known that the length of the flow-developing region in straight stretches of piping of circular section is given by Eq. (1) (Fox and Mc Donalds, 1985, Bejan. A., 1993, Geankoplis, 1993, Incropera and Dewitt, 1998, Welty et al, 2001). In this case, *Re* is the Reynolds number, which in itself brings the influence of the density, velocity and viscosity of the flowing fluid, and *D* is the diameter of the tube. For the case of non-circular sectioned pipe, the diameter shall be replaced by the hydraulic diameter, *Dh*.

$$L=0.05ReD \tag{1}$$

For curved tubes, Austing and Seader, 1974, proposed Eq. (2), which expresses the length in the form of the angle $\varphi$, which varies as a function of the Dean number, *De*, the radius of curvature of the tube, *R*, and the internal radius of it, *a*.

$$\varphi = 49\left(De\frac{a}{R}\right)^{0.33} \tag{2}$$

Springer et al., 2009, proposed Eq. (3), to predict the region of flow development of thin tubes in toroidal and helical formats, within the constraints $0 \leq Re \leq 400$; $0.25 \times 10^{-3}$ m $\leq 2a \leq 2 \times 10^{-3}$ m and $4 \times 10^{-3}$ m$\leq R \leq 32 \times 10^{-3}$ m.

$$L=0.322\ (2R)^{0.31}Re^{0.59}(2a)^{0.76} \tag{3}$$

This equation was adapted and tested by Amado et al., 2018a, in the form of Eq. (4), and presented reasonable suitability for symmetric bifurcations of rectangular sectioned microchannels, with angulation of 30 to 60 degrees, flow rates ranging from 1.39 x 10-10 $m^3$/s to 5.56 x 10-10 $m^3$/s and channel width of 80 to 200 µm, with water flowing under NTP conditions.

$$L=0.161\ (2R)^{0.31}Re^{0.59}(Dh)^{0.76} \tag{4}$$

As bifurcations are not curved tubes and therefore have no radius of curvature, the radius of an arc containing the bifurcation feeder channel and one of the outlets has been postulated in that paper, whose value is determined in Eq. (5).

$$R = 1200.5\frac{D_h Re^{0.66}}{\theta^2} \tag{5}$$

In Amado et al., 2018b, the same authors proposed Eq. (6) to describe flow phenomena in asymmetric bifurcations with constant half-angles as 45º and 30º, with circular-sectioned channels, with a diameter of 20 mm and a length of 0.9 m, varying flow rates from 5.56 x $10^{-10}$ $m^3/s$ to 2.78 x $10^{-9}$ $m^3/s$ of water in the NTP conditions. In this reference, they also propose Eq. (7), in the same bifurcations, but maintaining the constant flow rate in 1.39 x $10^{-9}$ $m^3/s$, with variation of combinations of pairs of half-angles between 15º and 90º.

$$L=0.23(2R)^{-0.1}Re^{-0.24}D^{1.1} \tag{6}$$

$$L=0.006111(2R)^{-0.1}Re^{-1.44}D^{1.1} \tag{7}$$

In Amado et al., 2018c, the authors supplemented the previous work with the variation of the canal diameter. They performed simulations via CFD, with widths between 10 mm and 35 mm, maintaining the same test conditions in which they arrived at the proposals of Eq. (6) and Eq. (7). Eq. (8) is the result of this investigation.

$$L=2.25(2R)^{-0.1}Re^{0.59}D^{1.1} \tag{8}$$

In the same paper, an equation was raised in which all the results presented in these last two works were taken into account. The result was Eq. (9).

$$L=2.69(2R)^{-0.1}Re^{0.59}D^{1.1} \tag{9}$$

In this sense, the proposal of this manuscript is to test Eq. (6) and Eq. (9) for flows that will vary the Reynolds number, not in the flow velocity, but in the properties "density and viscosity". The choice of Eq. (6) lies in the fact that it is an approach that ultimately varies *Re* and Eq (9) because it is a broad-ranging proposal that found good coincidence between simulated and calculated values, with the variation of all the parameters influencing the length *L*, within the same ranges of parameters used herein.

## 2. MATERIAL AND METHODS

If symmetric and asymmetric bifurcations are compared, according to the results presented in Amado et al., 2018a, b and c, the flow behavior and the consequent mode of calculating the length of the not developed flow region, are basically the same. It can be said that symmetrical bifurcations are just specific cases of asymmetric bifurcations. Thus, in order to generate two results in a single simulation, a standard asymmetric bifurcation of half angles $\theta_1$ = 30º and $\theta_2$ = 45º, with channels of 20 mm in diameter and outlets with length of 0.9 m was employed, as shown in Fig. 1.

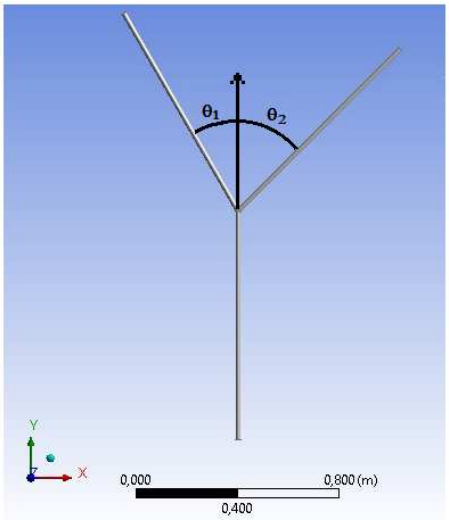


Figure 1. Sketch of asymmetric bifurcation, showing the half-angles $\theta_1$ and $\theta_2$ of each outlet.

Other researchers may question the legitimacy of testing *Re* again, since the flow variation is already a variation of this quantity. However, the authors' conclusions in their previous works are restricted to water flowing inside the bifurcations. The authors believe that the flow of more viscous and less dense fluids should be tested for those equations, because intuitively it is to be assumed that such quantities influence the flow development at the entrance of the branches.

Another important observation is that the low values of *Re* employed in this manuscript are due to the fact that this research was initiated in Amado et al 2018a with bifurcations made of microchannels, which demanded low values of flow rate. To keep comparison basis, the authors continued in this paper with *Re* values on the same level as those.

### 2.1 Simulation strategy

Similar to what was done by Amado et al, 2018a, equations that govern the phenomenon, represented here between (10) and (12), were discretized in finite differences for two dimensions. This numerical method was chosen due to the simplicity of the geometry where the fluid flows, which does not demand a robust numerical tool. The two sides of the fork were separated and treated as single conduits, with initial velocity condition determined by Eq. (13). A non-uniform structured mesh was used in the axial direction (z) and uniform in the transverse direction (x). Axially, 260 divisions were made, with 60 lines in the initial 5% of the conduit and 200 lines in the remaining 95%. For the case of oils with high viscosity or low density, more refinement of the axial mesh was required at the entrance of each side of the bifurcations and 120 divisions were made in the initial 2%, remaining the 200 lines for the remainder. Transversally, 1200 divisions were made, equally distributed. Fig. 2a shows a sketch of the generated mesh. This structuring allowed to concentrate the mesh at the beginning of the bifurcation and to gain time of computational processing, in such a way that for each simulation were spent about 15 hours. Exception to oils of high viscosity, such as hydraulic ones, or low density, such as lubricants, where eventually the simulations took up to 28 hours. Homogeneous distributions, with uniform structured meshes in both directions were attempted, but took 3 days to complete and were discarded. The simulated time periods ranged from 1 to 1000 seconds, with varying steps, where there was no relevant difference between the results and 1 second with time step of 2 x $10^{-5}$ s was taken as sufficient and representative of the real phenomenon. The convergence criterion adopted was $10^{-9}$, compared to the relative error between two adjacent nodes.

In order to certify if the constructed images were coherent, the same simulation was performed in a commercial package. Considering this certification, the simulation of the processes was taken as a parameter of comparison for the values calculated by Eq. (6) and (9). Fig. 2b shows the mesh generated by the commercial code.

Equation for mass conservation:

$$\frac{\partial v_x}{\partial x} + \frac{\partial v_y}{\partial y} = 0 \tag{10}$$

*x* Momentum:

$$\rho\left(\frac{\partial v_x}{\partial t} + v_x\frac{\partial v_x}{\partial x} + v_z\frac{\partial v_x}{\partial z}\right) = \rho g_x - \frac{\partial P}{\partial x} + \mu\left(\frac{\partial^2 v_x}{\partial x^2} + \frac{\partial^2 v_x}{\partial z^2}\right) \tag{11}$$

*z* Momentum:

$$\rho\left(\frac{\partial v_z}{\partial t} + v_x\frac{\partial v_z}{\partial x} + v_z\frac{\partial v_z}{\partial z}\right) = \rho g_z - \frac{\partial P}{\partial z} + \mu\left(\frac{\partial^2 v_z}{\partial x^2} + \frac{\partial^2 v_z}{\partial z^2}\right) \tag{12}$$

$$v_{axial} = \frac{2Q}{\pi r_1^4}(a^2 - r^2) \pm \cos\theta_i \tag{13}$$

The shape of the region of flow development in view of the velocity field as a “topographical relief” was shown by Amado et al., 2018a, represented here as Fig. 3. In vector terms, Gongnan et al., 2014, studying zero-angled bifurcations, established Fig 4. In the present work, based on the simulation model developed in Amado et al, 2018a, it is important to show the velocity field in vector terms, which is measured to reach the value of the length *L*, and in relief represented by colors, according to Fig. 5, which demonstrate the flow in one of the outlets of a bifurcation in a tube with diameter 0,01 m.

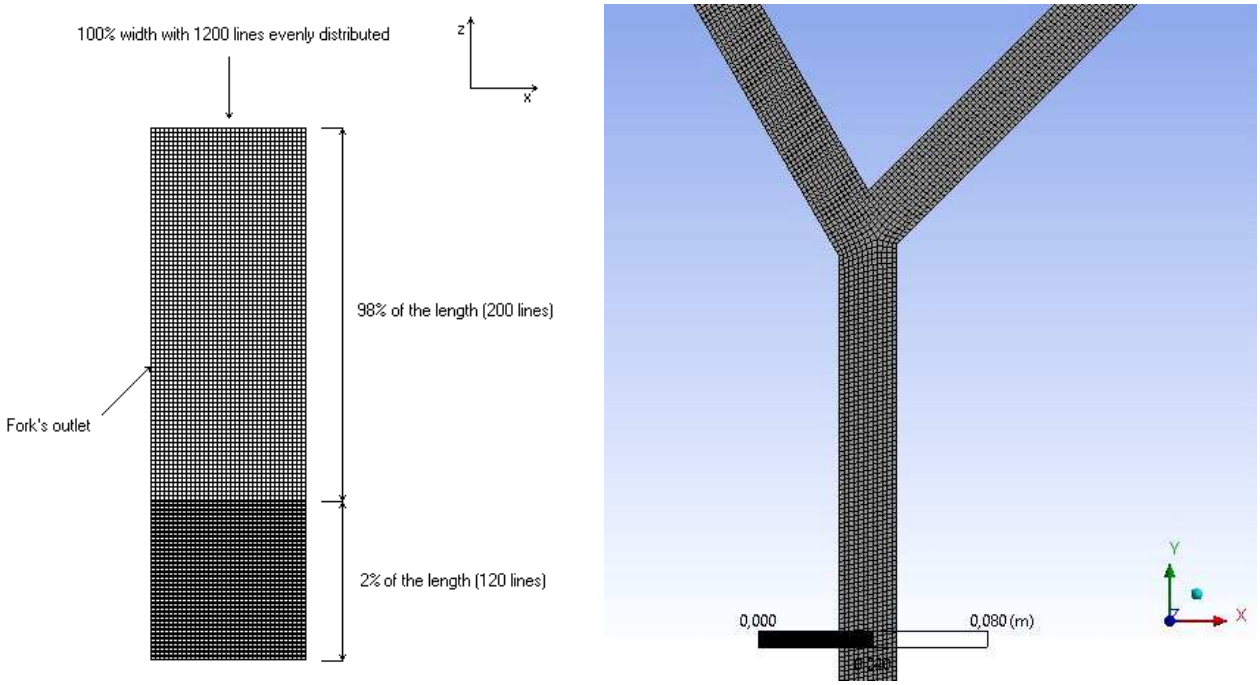


(a) (b)

Figura 2. (a) Sketch of the non-uniform structured mesh in the axial direction (z) and uniform in the transverse direction (x), for the simulation in finite differences, at one of the bifurcation outlets and (b) The mesh in the commercial package was due to its internal methods. In this example, 21041 nodes and 19408 elements were generated.

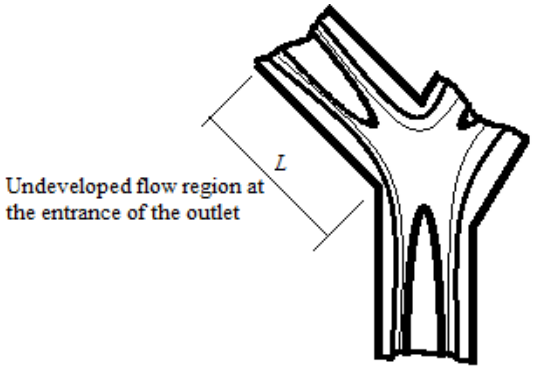


Figure 3. Scheme according to Amado et al, 2018a, showing the length of the turbulence region, in terms of the velocity field as a "topographical relief".

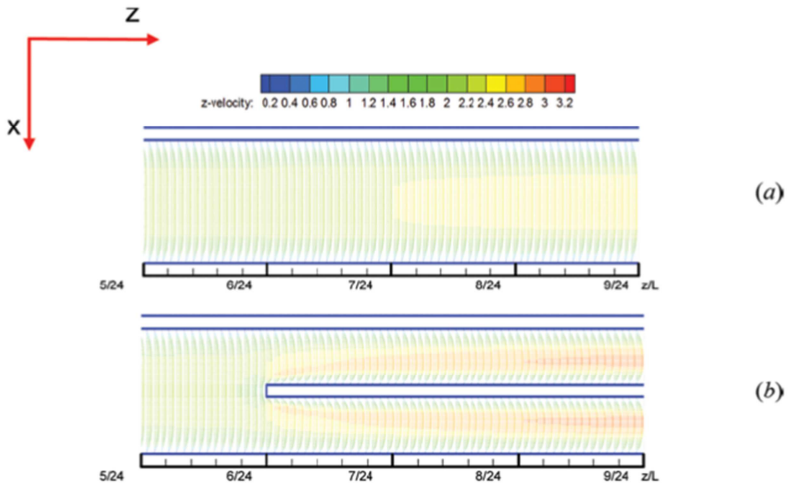


Figure 4. Symmetric zero-angled bifurcation, in a study developed by Gongnan et al, 2014, showing the vector field of velocities caused by the obstacle.

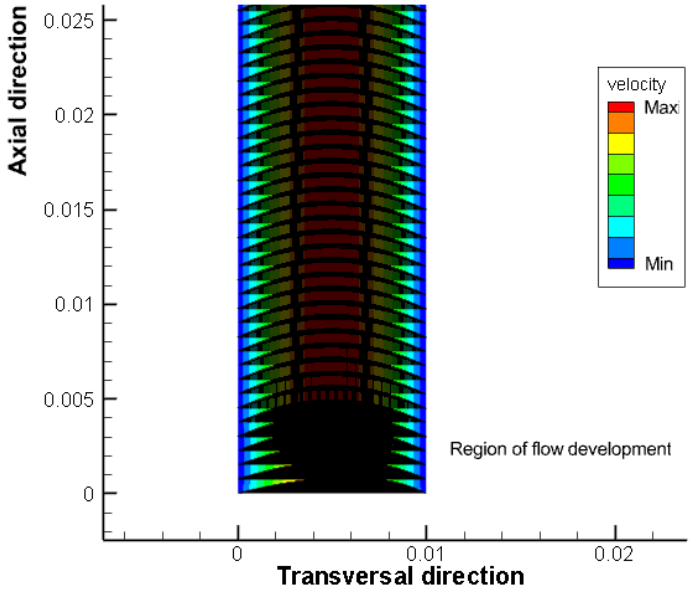


Figure 5. Velocity field shown in vector terms and color distribution. Colors show the relief highlighted in Fig. 2.

## 2.2 Physical properties

To verify the behavior of the flow developing region for low Reynolds numbers, four types of oil were selected from public data available in commercial catalogs and on the internet. Respectively, Tab. 1 to 4 set forth the viscosity, density and Reynolds number values for biodiesel oils, edible oils, hydraulic oils and lubricating oils, with flow rate of $1{,}39x10^{-10}$ $m^3/s$, in NTP conditions.

Important assumptions for the use of physical properties and development of the work were:

a) Viscosity was that provided in catalogs, usually measured at 40 $^oC$;
b) Density reported in the catalogs was considered compatible for viscosity temperature and Reynolds number calculation;
c) When the catalog provided only the values of kinematic viscosity (case of hydraulic oils), the average density of 878 $kg/m^3$ was adopted as the standard;
d) The variation of the values of *Re* were the focus and therefore more important than the absolute values of viscosity and density. It means that, for purposes of this study the verification of the length of the region of flow development is more important than the fidelity to the real values of these physical properties;

Each of the rows in the following tables relate to a simulation performed. Images were generated, where the length of the region of interest was measured, similar to the methodology developed in Amado et al, 2018a, b and c.

Table 1. Physical properties of biodiesel oils

| Outlet | Oil type | Viscosity 40 $^oC$ (kg/ms) | Density | Reynolds Number |
|---|---|---|---|---|
| Left 1 | Conventional Diesel | 0.00550208 | 859.7 | 0.006913293 |
| Right1 | Conventional Diesel | 0.00550208 | 859.7 | 0.006913293 |
| Left 2 | Castor Biodiesel | 0.00525000 | 875.0 | 0.007374179 |
| Right 2 | Castor Biodiesel | 0.00525000 | 875.0 | 0.007374179 |
| Left 3 | Babassu Biodiesel | 0.00449800 | 865.0 | 0.008508668 |
| Right 3 | Babassu Biodiesel | 0.00449800 | 865.0 | 0.008508668 |
| Left 4 | Piqui Biodiesel | 0.00345735 | 886.5 | 0.011344891 |
| Right 4 | Piqui Biodiesel | 0.00345735 | 886.5 | 0.011344891 |
| Left 5 | Cotton Biodiesel | 0.00296870 | 960.0 | 0.014307701 |
| Right 5 | Cotton Biodiesel | 0.00296870 | 960.0 | 0.014307701 |
| Left 6 | Palm Biodiesel | 0.00258309 | 849.7 | 0.014554301 |
| Right 6 | Palm Biodiesel | 0.00258309 | 849.7 | 0.014554301 |

Table 2. Physical properties of edible oils

| Outlet | Oil type | Viscosity 40 $^{o}$C (kg/ms) | Density (kg/m$^3$) | Reynolds Number |
|---|---|---|---|---|
| Left 7 | Avocado | 0.00442042 | 873.6 | 0.008744086 |
| Right 7 | Avocado | 0.00442042 | 873.6 | 0.008744086 |
| Left 8 | Sunflower | 0.00390320 | 873.2 | 0.009898227 |
| Right 8 | Sunflower | 0.00390320 | 873.2 | 0.009898227 |
| Left 9 | Soy | 0.00382539 | 879.4 | 0.010171281 |
| Right 9 | Soy | 0.00382539 | 879.4 | 0.010171281 |
| Left 10 | Cotton | 0.00369643 | 871.8 | 0.010435159 |
| Right 10 | Cotton | 0.00369643 | 871.8 | 0.010435159 |
| Left 11 | Canola | 0.00357979 | 877.4 | 0.010844381 |
| Right 11 | Canola | 0.00357979 | 877.4 | 0.010844381 |

Table 3. Physical properties of hydraulic oils

| Outlet | Oil type | Viscosity 40 $^{o}$C (kg/ms) | Density (kg/m$^3$) | Reynolds Number |
|---|---|---|---|---|
| Left 20 | ISO VG 10 | 0.00878000 | Average value of 878.0 | 0.004424507 |
| Right 20 | ISO VG 10 | 0.00878000 | | 0.004424507 |
| Left 21 | ISO VG 7 | 0.00597040 | | 0.006506629 |
| Right 21 | ISO VG 7 | 0.00597040 | | 0.006506629 |
| Left 22 | ISO VG 5 | 0.00403880 | | 0.009618494 |
| Right 22 | ISO VG 5 | 0.00403880 | | 0.009618494 |
| Left 23 | ISO VG 3 | 0.00289740 | | 0.013407598 |
| Right 23 | ISO VG 3 | 0.00289740 | | 0.013407598 |
| Left 24 | ISO VG 2 | 0.00193160 | | 0.020111397 |
| Right 24 | ISO VG 2 | 0.00193160 | | 0.020111397 |
| Left 25 | ISO VG S | 0.00131700 | | 0.029496716 |
| Right 25 | ISO VG S | 0.00131700 | | 0.029496716 |

Table 4. Physical properties of lubricating oils

| Outlet | Oil type | Viscosity 40 $^{o}$C (kg/ms) | Density (kg/m$^3$) | Reynolds Number |
|---|---|---|---|---|
| Left 12 | SAE 60 | 0.0037000 | 154.17 | 0.001229056 |
| Right12 | SAE 60 | 0.0037000 | 154.17 | 0.001843585 |
| Left 13 | SAE 50 | 0.0037000 | 193.71 | 0.002316409 |
| Right 13 | SAE 50 | 0.0037000 | 193.71 | 0.002316409 |
| Left 14 | SAE 40' | 0.0037000 | 256.94 | 0.003072521 |
| Right 14 | SAE 40' | 0.0037000 | 256.94 | 0.003072521 |
| Left 15 | SAE 40 | 0.0029000 | 201.39 | 0.003072592 |
| Right 15 | SAE 40 | 0.0029000 | 201.39 | 0.003072592 |
| Left 16 | SAE 30 | 0.0029000 | 266.06 | 0.004059257 |
| Right 16 | SAE 30 | 0.0029000 | 266.06 | 0.004059257 |
| Left 17 | SAE 20 | 0.0026000 | 348.99 | 0.005938880 |
| Right 17 | SAE 20 | 0.0026000 | 348.99 | 0.005938880 |

## 3. RESULTS AND DISCUSSION

Figure 6 shows a flow simulation performed through the commercial code. Fig. 7 shows the same phenomenon, however, simulated by the finite difference method. In this last figure, it can be seen how the length in the generated image was measured. As said before, the commercial package simulation was done to compare only the aspect and so, to ensure the effectiveness of non-commercial simulation.

Figures 8 to 11 show graphs with the comparisons between the amounts relative to values measured and predicted by Eq. (6) and (9), for each type of oil tested.

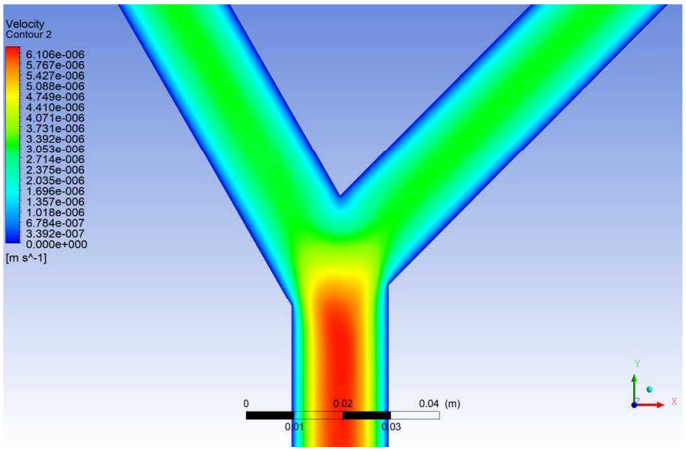


Figure 6. Simulation of the soybean oil flow, according to the data shown in Table 2, bifurcation 9.

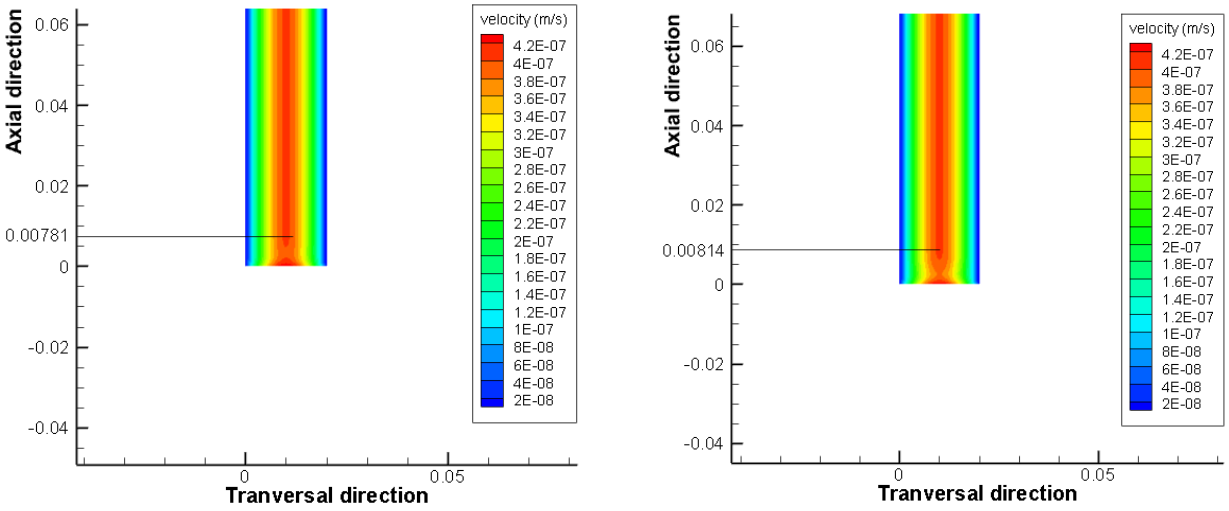


Figure 7. Images generated from simulation in finite differences method, according to the data shown in Tab. 2, bifurcation 9. Measurement of the undeveloped flow region was performed on the image as shown.

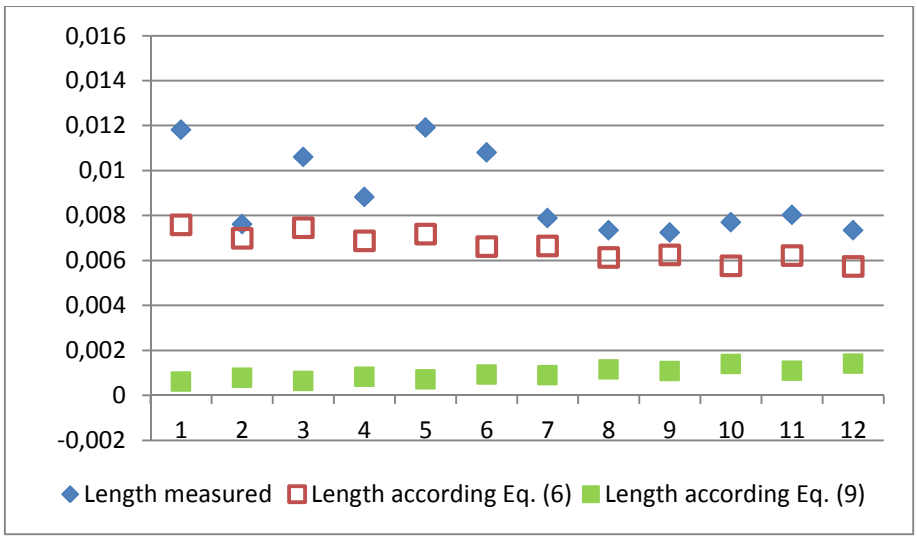


Figure 8. Comparison between measured values for biodiesel oils and values calculated by equations (6) and (9)

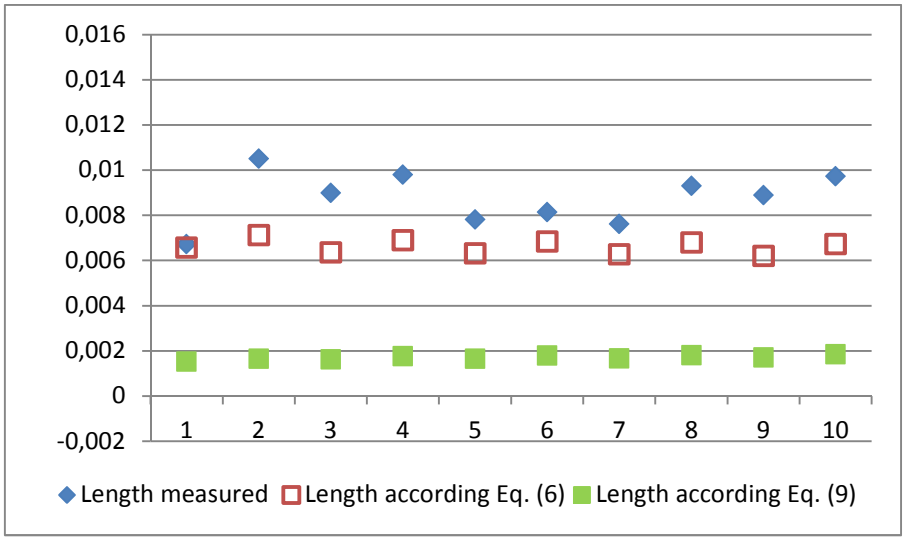


Figure 9. Comparison between measured values for edible oils and values calculated by equations (6) and (9)

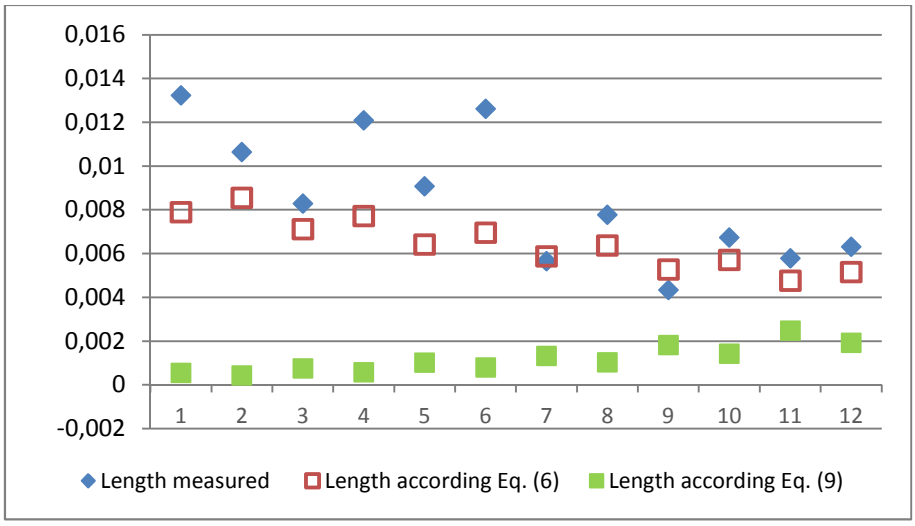


Figure 10. Comparison between measured values for hydraulic oils and values calculated by equations (6) and (9)

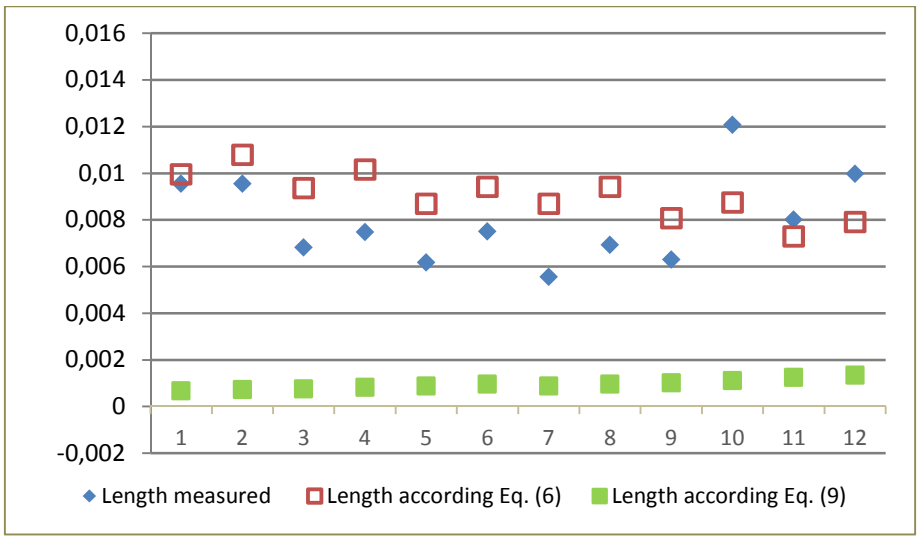


Figure 11. Comparison between measured values for lubricant oils and values calculated by equations (6) and (9)

The observation of the figures that represent the comparison between measured values and values calculated by Eq. (6) and (9), shows that Eq. (6) was much better for biodiesel oils, edible oils, higher density lubricating oils (266.06 $m^3$/kg to 348.99 $m^3$/kg) and higher viscosity hydraulic oils (0.00289740 kg/ms to 0.0087800 kg/ms). Measured values presented some scattering, but, as a rule, were reasonably well predicted by this expression. Eq. (6) was developed to represent the values of variation of water flow rate in the NTP conditions, but this, in the last analysis, represents a variation in the Reynolds Number, which is exactly the case in the current paper.

In the case of low-viscosity hydraulic oils (ranging from 0.001317 kg/ms to 0.0019316 kg/ms), Eq. (9) behaved a little better, i.e., when compared to its own behavior in relation to other conditions. This expression was postulated by Amado et al, 2018c, to represent wide variation relative to water flowing under NTP conditions, but in their manuscript, showed excessive spreading and moderate congruence. In the present case, it was also less adequate, but in case where there was good match, it showed better coincidence than the results presented in that paper.

In all cases, the higher values of *Re* presented better coincidences between measured and calculated.

The influence of *Re* on ramified structures was also observed by Almeida et al, 1999, who studied widely branched trees. They showed that the larger the number of branches, the more the flow distribution depends on the larger Reynolds numbers. In the same way, it finds support in Mauroy et al, 2003, who affirm that the flow distribution at the outlets depends very much on the Reynolds number and on the geometry of the ramified structure. Similarly, Poole et al., 2014, studying cross-slot flow phenomena, stated that the intensity of the Reynolds number influences the flow aspect at the outlets.

The present work closes a cycle of construction of equations that try to predict the size of the region of flow development in bifurcations. The next step proposed by the author will be the prediction of the extension of the region of thermal development, evinced by Ghobadi and Muzychka, 2016, as a subject of still little research.

An important and final observation to be made is that a more accurate survey would require an experimental apparatus in which the region of interest could be measured visually. For example, a bifurcation made with a glass tube, feed with water from a raised box, having a fluid circulation pump, could compose a laboratory scheme for actual surveys and thus corroborate the mathematical results proposed herein. It is suggested that future investments take this infrastructure into account.

## 4. CONCLUSIONS

Equations presented in previous works, designed to predict the length of the region of flow development in bifurcations, were tested by CFD, under conditions of variation of low Reynolds number, specifically in the properties viscosity and density. Four sets of oils (biodiesel, edible, hydraulic and lubricating) were selected, with absolute viscosities ranging from 0.00193160 kg/ms to 0.0597040 kg/ms, as well as density ranging from 154.17 kg/$m^3$ to 960 kg/$m^3$, which resulted in *Re* strictly laminate, varying between 0.006506629 and 0.010171281.

The equation in the format $L = 2.69\ (2R)^{-0.1} Re^{0.59} D^{1.1}$, considered broad-spectrum, developed by Amado et al 2018c, found reasonable match only for low viscosity hydraulic oils. On the other hand, the equation in the format $L = 0.23(2R)^{-0.1} Re^{-0.24} D^{1.1}$, specific for flow rate variation, developed by Amado et al 2018b, for water flowing in the NTP conditions, which ultimately also represents a variation of Reynolds number, showed good coincidence of values for most of the cases and proved to be applicable to the boundary conditions and physical properties used in the present work. In all cases, the higher values of Reynolds number, *Re*, presented better coincidences between measured and calculated.

## 5. ACKNOWLEDGEMENTS

The authors acknowledge “Programa Pesquisa Produtividade - Universidade Estácio de Sá (PPP-UNESA)” and “Programa de Iniciação Científica – Universidade Estácio de Sá (PIC-UNESA)”, for funding the research.

## 6. REFERENCES

Almeida, M., Andrade, J., Buldyrev, S., Cavalcante, F., Stanley, H., & Suki, B., 1999. “Fluid flow through ramified structures”. *Physical Review E*, 60(5), 5486–5494. DOI: 10.1103/PHYSREVE.60.5486;

Amado, F. P., Avelino. M. R., Colman, J., Lucena, E. S., Mazzarela, N. G. S., 2018a. “Developing Flow in the Inlet Region of Bifurcations in Microchannels with Symmetric Angulation”. *in the Proceedings of the Comgresso Brasileiro de Engenharia Mecãnica - CONEN2018*, Salvador, BA, Brasil. DOI: 10.26678/ABCM.CONEM2018.CON18-0253;

Amado, F. P., Avelino. M. R., Colman, J., Lucena, E. S., Mazzarela, N. G. S., 2018b. “Forecasting the Length of the Undeveloped Flow Region in the Inlet of Asymmetric Bifurcations I”. *In the Proceedings of the 17th Brazilian Congress of Thermal Sciences and Engineering - ENCIT2018*, Águas de Lindóia, SP, Brazil. DOI://10.26678/ABCM.ENCIT2018.CIT18-0008;

Amado, F. P., Avelino. M. R., Colman, J., Lucena, E. S., Mazzarela, N. G. S., 2018c. "Forecasting the Length of the Undeveloped Flow Region in the Inlet of Asymmetric Bifurcations II". *In the Proceedings of the 17th Brazilian Congress of Thermal Sciences and Engineerings - ENCIT2018*, Águas de Lindóia, SP, Brazil. DOI://10.26678/ABCM.ENCIT2018.CIT18-0009;

Austin, L. R., Seader, J. D., 1974. "Entry Region for Steady Viscous Flowing Coiled Circular Pipes". American Institute of Chemical Engineers. vol 20. pp 820–822;

Bejan, A., 1993. "Heat Transfer". John Wiley & Sons. Inc., p. 292;

Gongnan, X., Shian, L., Bengt S., Weihong, Z., and Haibin, L., 2014, "A numerical study of the thermal performance of microchannel heat sinks with multiple length bifurcation in laminar liquid flow", *Numerical Heat Transfer, Part A*, 65: 107–126, DOI: 10.1080/10407782.2013.826084.

Fox and Mc Donald., 1985. "Introduction to Fluid Mechanics". Jonh Wiley & Sons, 3a ed.;

Geankoplis, C.J., 1993. "Transport Processes and Unit Operations". 3rd Edition. Prentice-Hall, Inc.;

Incropera, F.P. e DeWitt, D.P., 1998, "Fundamentos da Transferência de Calor e de Massa". 4a Edição. LTC Livros Técnicos, Rio de Janeiro, Brazil;

Ghobadi. M., Muzychka, Y. S., 2016, "A Review of Heat Transfer and Pressure Drop Correlations for Laminar Flow in Curved Circular Ducts", *Heat Transfer Engineering*, 37:10, 815-839, DOI: 10.1080/01457632.2015.1089735;

Mauroy, B., Filoche, M., Andrade, J., & Sapoval, B. 2003. "Interplay between Geometry and Flow Distribution in an Airway Tree". *Physical Review Letters*, 90(14). DOI: 10.1103/PHYSREVLETT.90.148101

Poole, R, J., Rocha, G. N., Oliveira,P., J., A, 2014,. "A symmetry-breaking inertial bifurcation in a cross-slot flow", *Computers & Fluids 93*, pp 91-99. DOI: 10.1016/J.COMPFLUID.2014.01.008

Springer, F., Carretier, E., Veyret, D., Moulin, P., 2009. "Developing Lengths in Woven and Helical Tubes with Dean Vortices Flows". *Engineering Applications of Computational Fluid Mechanics*. 3:1. pp. 123-134. DOI:10.1080/19942060.2009.11015259;

Welty, J.R., Wicks, C.E., Wilson, R.E., Rorrer, G., 2001. "Fundamentals of Momentum, Heat, and Mass Transfer". 4th Ed. John Wiley & Sons.

## 7. RESPONSIBILITY NOTICE

The authors are the only responsible for the printed material included in this paper.